

Classification: Chemistry

## **Dynamics of photogenerated holes in surface modified $\alpha$ -Fe<sub>2</sub>O<sub>3</sub> photoanodes for solar water splitting**

Monica Barroso,<sup>a1</sup> Camilo Mesa, Stephanie R. Pendlebury,<sup>a</sup> Alexander J. Cowan,<sup>a</sup> Takashi Hisatomi,<sup>b</sup> Kevin Sivula,<sup>b</sup> Michael Grätzel,<sup>b</sup> David R. Klug,<sup>a</sup> James R. Durrant<sup>a1</sup>

<sup>a</sup>*Department of Chemistry, Imperial College London, South Kensington Campus, London SW7 2AZ, United Kingdom*

<sup>b</sup>*Ecole Polytechnique Fédérale de Lausanne, Laboratoire de Photonique et Interfaces, CH-1015 Lausanne, Switzerland*

<sup>1</sup>To whom correspondence should be addressed:

[m.barroso@imperial.ac.uk](mailto:m.barroso@imperial.ac.uk)

[j.durrant@imperial.ac.uk](mailto:j.durrant@imperial.ac.uk)

Author contributions: M.B and J.R.D. designed research; M.B, C.M and S.R.P. performed research and analyzed data; A.J.C. and D.R.K contributed analytic tools K.S., T.H and M.G contributed new reagents; M.B and J.R.D. wrote the paper.

Keywords: Hematite, Water Splitting, Cobalt Oxide, Surface States, Transient Absorption Spectroscopy

## **Abstract**

This paper addresses the origin of the decrease in the external bias required for water photoelectrolysis with hematite photoanodes, observed following surface treatments of such electrodes. We consider two alternative surface modifications: a cobalt oxo/hydroxo-based ( $\text{CoO}_x$ ) overlayer, reported previously to function as an efficient water oxidation co-catalyst, and a  $\text{Ga}_2\text{O}_3$  overlayer, reported to passivate hematite surface states. Transient absorption studies of these electrodes under applied bias showed that the cathodic shift of photocurrent onset observed after each of the surface modifications is accompanied by a similar cathodic shift of the appearance of long-lived hematite photoholes, due to a retardation of electron / hole recombination. The origin of the slower electron / hole recombination is assigned primarily to enhanced electron depletion in the  $\text{Fe}_2\text{O}_3$  for a given applied bias, consistent with the elimination of surface states and the associated Fermi level pinning.

## Introduction

Efficient hydrogen generation from solar water splitting in a photoelectrochemical (PEC) cell using at least one photoactive semiconductor electrode has been target of research for several decades.(1-4) Considerable progress is being made in the development of suitable electrodes for this solar driven fuel synthesis.(5-8) One class of photoelectrode materials attracting particular interest for this purpose is metal oxides, including  $\text{TiO}_2$ ,  $\text{WO}_3$ ,  $\text{BiVO}_4$  and  $\text{Fe}_2\text{O}_3$ .(1, 9-13) Such metal oxides are attractive due to their stability, low cost, semiconducting properties and, for some of these oxides, strong visible light absorption. However a major limitation for the application of such oxides in solar driven water splitting is that they typically require an additional electrical bias to achieve both the water oxidation and reduction reactions simultaneously under solar irradiation. This limitation is particularly severe for the lower optical bandgap oxides, such as  $\text{Fe}_2\text{O}_3$  and  $\text{BiVO}_4$ .(10, 12) which are of interest due to their enhanced absorption of solar irradiation. The development of strategies to reduce or remove this electrical bias requirement is therefore a key target of ongoing research.(14, 15)

One strategy, which has been shown to reduce electrical bias required to achieve solar driven water splitting on such metal oxides, has been the deposition of surface overlayers on the light absorbing photoelectrode. Interest has recently focused upon in-situ deposition of cobalt oxo/hydroxo-based ( $\text{CoO}_x$ ) overlayers on several water oxidation photoanodes,(15-20) building upon recent reports that such amorphous  $\text{CoO}_x$  layers formed from Co(II) salts are effective water oxidation electrocatalysts, operating at moderate overpotentials.(21) The deposition of a range of other catalytic and non-catalytic materials have also been shown to reduce the electrical bias required for solar driven water oxidation, including other cobalt-based treatments,(22)  $\text{IrO}_2$  nanoparticles(23) and  $\text{Ga}_2\text{O}_3$  and  $\text{Al}_2\text{O}_3$  overlayers.(24-26) At present, the functional origin of the reduced requirement for electrical bias achieved by these deposition treatments has not been unambiguously established. In some cases this has been suggested to result from catalytic function enhancing the water oxidation kinetics / reducing the overpotential required to drive water oxidation.(15, 18) In other cases, the treatments have been suggested to passivate surface states, reducing the kinetics of surface recombination reactions.(24, 25)

In this paper we report a transient absorption and spectroelectrochemical study of the dynamics of photogenerated charge carriers in the two composite photoelectrodes, in operating conditions (i.e, under external bias control). On the basis of these studies, we suggest that the performance enhancement observed following such treatments is largely a consequence of enhanced electron depletion in the photoelectrode under applied bias, resulting in a reduction of electron / hole recombination losses.

We focus herein upon the water photo-oxidation properties of hematite photoelectrodes before and after two alternative surface modifications, with  $\text{CoO}_x$  and  $\text{Ga}_2\text{O}_3$ . Electrodeposition of an amorphous  $\text{CoO}_x$  from  $\text{Co(II)}$  salts in an aqueous phosphate buffer has been shown to form an electrochemical water oxidation catalyst (Co-Pi) on ITO.(21) In contrast  $\text{Ga}_2\text{O}_3$  is a wide bandgap oxide not thought to be catalytic for water oxidation. Surface modification of hematite photoanodes with either of these materials have been shown to reduce by 100-200 mV the electrical bias required to enable water photo-oxidation.(18, 25)

Hematite is particularly interesting material for solar water splitting due to its relatively small bandgap (2.1 eV), chemical stability, widespread availability and facile preparation by scalable methods.(12) In common with most of the oxide materials of interest for photoelectrochemical water photolysis, hematite is an n-type semiconductor. The presence of oxygen vacancies in the lattice of hematite, which are compensated by  $\text{Fe}^{2+}$  ions, results in the intrinsic n-type conductivity of this material.(27, 28) Due to this intrinsic n-type doping, solar water splitting strategies with hematite have mostly employed this material as an oxidation photoelectrode, with photogenerated electrons being transported through the electrode to a back contact and then transferred to a counter electrode (typically platinum) to achieve water reduction and thus hydrogen generation.(12, 29, 30) A range of n-type dopants (e.g. silicon and niobium)(22, 31) have been shown to enhance the photoelectrode performance, typically assigned to improved electron conduction to the back contact.(22) In addition, nanostructuring has also been shown to enhance photocurrent generation, assigned to increasing the efficiency of hole transfer to the electrode surface for water oxidation. Typically, in a photoelectrochemical (PEC) cell an electrical bias is applied between the oxidation and reduction electrodes. This bias is in part required as the conduction band of hematite lies below the water reduction

potential, with photogenerated electrons therefore requiring an additional electrical bias to achieve proton reduction. An additional role of the applied bias has been shown to be the achievement of partial depletion of electrons from the hematite film, thereby increasing the lifetime of photogenerated holes (the minority charge carrier in these films)(32, 33). For flat photoelectrodes, this electron depletion corresponds to the formation of a surface space charge layer, and the associated band bending towards the electrode surface. For nanostructured or very thin films, where the feature size may be comparable to the depletion depth (as is probably the case for the films employed herein), this band bending may be less pronounced, and the applied bias rather reduces the (dark) electron density throughout most of the film.

We have recently shown that observation of water photo-oxidation by several oxide photoelectrodes is strongly correlated with the yield of long-lived (100 ms – seconds) photogenerated holes observed in transient optical measurements. This correlation was observed for a range of oxides ( $\text{TiO}_2$ ,  $\text{WO}_3$  and  $\text{Fe}_2\text{O}_3$ ), for both flat and nanostructured films, and both under electrical bias control and in the presence of chemical electron scavengers.(32, 34-36) Most recently, we have demonstrated that  $\text{CoO}_x$  coupled to a hematite film resulted in the generation of long lived-holes in the absence of applied bias, indicating that this treatment resulted in a significant reduction in electron / hole recombination losses in such films.(20) In this paper, we extend these studies to consideration of the water photo-oxidation function of hematite photoelectrodes following surface treatments with  $\text{CoO}_x$  and  $\text{Ga}_2\text{O}_3$  overlayers. These photoanode systems,  $\text{Fe}_2\text{O}_3/\text{CoO}_x$  and  $\text{Fe}_2\text{O}_3/\text{Ga}_2\text{O}_3$ , have been discussed recently and are representative examples of surface modifications with ascribed catalytic and surface passivation roles, respectively.(18, 25) For that reason, these model systems were investigated under applied bias corresponding to photoelectrochemical device function, with the purpose of gaining new insights into how surface modifications can produce an enhancement in photoelectrode performance.

## Results

Two types of mesoporous hematite films and surface overlayer treatments were considered in this study. The first type, silicon-doped  $\alpha\text{-Fe}_2\text{O}_3$  grown by an

atmospheric pressure vapour deposition (APCVD) technique (hereafter designated APCVD hematite), exhibits a cauliflower-like nanostructure with feature sizes in the order of 5-10 nm, and has recently demonstrated the highest solar water oxidation photocurrents for an oxide-based photoanodes tested under standard conditions.(23) A thin layer of amorphous  $\text{CoO}_x$  was electrodeposited on the surface of these photoanodes from a  $\text{Co(II)}$  solution in aqueous phosphate buffer. For the second type of electrodes, ultrathin hematite films ( $\sim 20$  nm) were prepared by ultrasonic spray pyrolysis (USP) (hereafter designated USP hematite).(37) These electrodes were subsequently modified with a  $\text{Ga}_2\text{O}_3$  overlayer by chemical bath deposition (CBD).(25) The choice of USP films instead of the better performing APCVD for the investigation of the role of  $\text{Ga}_2\text{O}_3$  is due to the detrimental effect that CBD deposition conditions have on the quality of films prepared by APCVD.(25) Ultrathin USP deposited films were preferred in order to enhance the effect of  $\text{Ga}_2\text{O}_3$  modification.

Both the  $\text{CoO}_x$  and  $\text{Ga}_2\text{O}_3$  treatments resulted in cathodic shifts of the water oxidation photocurrent onset by more than 100 mV (Figure 1), consistent with previous observations.(18, 25) We note that, in contrast, a cathodic shift of the dark current was observed with the Co-Pi treatment while an anodic shift was observed with the  $\text{Ga}_2\text{O}_3$  modification, consistent with the corresponding water oxidation catalytic activities.(25, 38) Photocurrent measurements under chopped illumination (Figure S1) show a cathodic shift of the transient charging currents at modest applied bias for both treatments, assigned to the passivation of surface trapping sites by these treatments.(18, 25, 26) In addition we note that neither surface modification resulted in a significant shift in the onset of photocurrent transients, in agreement with previous observations,(17, 19) suggesting that these treatments do not change the flat band potential of the electrode. We have reported qualitatively similar photocurrent onset shifts with  $\text{CoO}_x$  treatment of USP hematite photoanodes(20) and have observed similar trends upon  $\text{Co}^{2+}$  adsorption of APCVD and ultrathin USP hematite used in this study. Furthermore, surface adsorption of  $\text{Co}^{2+}$  on  $\text{Ga}_2\text{O}_3$  modified photoanodes produced an additional cathodic shift of the photocurrent onset, confirming the cumulative enhancement of photoelectrochemical performance caused by the two modifications (Figure S2).(25)

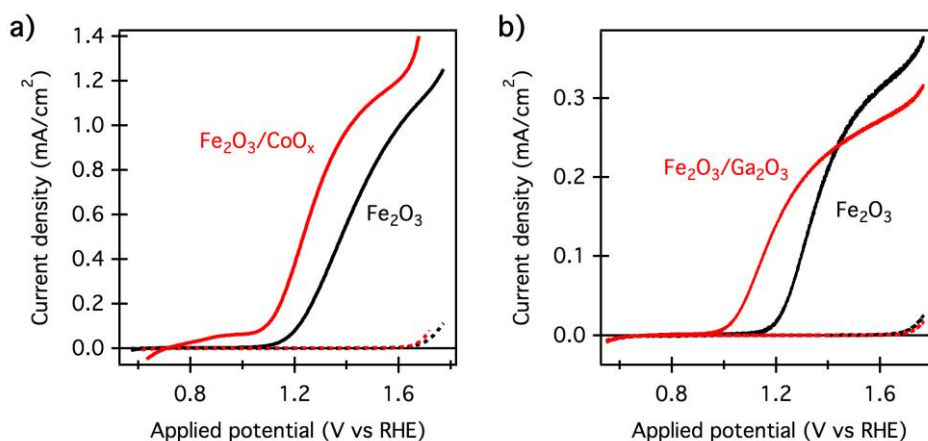


**Figure 1.** Photocurrent-potential curves of mesoporous hematite photoanodes before and after surface modification. a) APCVD hematite without (black) and with (red)  $\text{CoO}_x$  overlayer; b) Ultrathin USP hematite without (black) and with (red)  $\text{Ga}_2\text{O}_3$  overlayer. Measurements in 0.1 M NaOH (pH 12.6), at  $10 \text{ mV s}^{-1}$ , in dark (dashed lines) and illuminated with simulated sunlight ( $\sim 1 \text{ Sun}$ , AM 1.5G) through the electrolyte-electrode (EE) interface.

We turn now to consideration of the impact of these two surface modifications upon the kinetics of photogenerated charge carriers. Figure 2 shows transient absorption data observed following low intensity pulsed excitation at 355 nm in the absence of an external bias. The data monitors the photoinduced absorption at 700 nm, representative of the broad photoinduced absorption observed between 550 and 900 nm previously assigned to photogenerated  $\text{Fe}_2\text{O}_3$  holes due to the faster decay rate of these transients in the presence of methanol.(32) The decay kinetics of these photoholes in untreated APCVD and USP hematite are very similar. It is apparent that the  $\text{CoO}_x$  treatment results in a very significant (3 orders of magnitude) increase in the lifetime of these photogenerated holes, as we have reported previously.(20) A smaller increase in the hole lifetime is also observed when the hematite photoanode is modified by surface adsorption of  $\text{Co}^{2+}$  ions (Figure S3). In contrast, the  $\text{Ga}_2\text{O}_3$  treatment does not significantly increase the hole lifetime in the absence of applied bias. We have previously assigned the retardation of electron / hole recombination following  $\text{CoO}_x$  treatment to an enhancement of electron depletion in the hematite film promoted by the  $\text{Fe}_2\text{O}_3/\text{CoO}_x$  heterojunction formed.(20) It is apparent that, without external bias, the  $\text{Ga}_2\text{O}_3$  deposition does not cause such electron depletion.

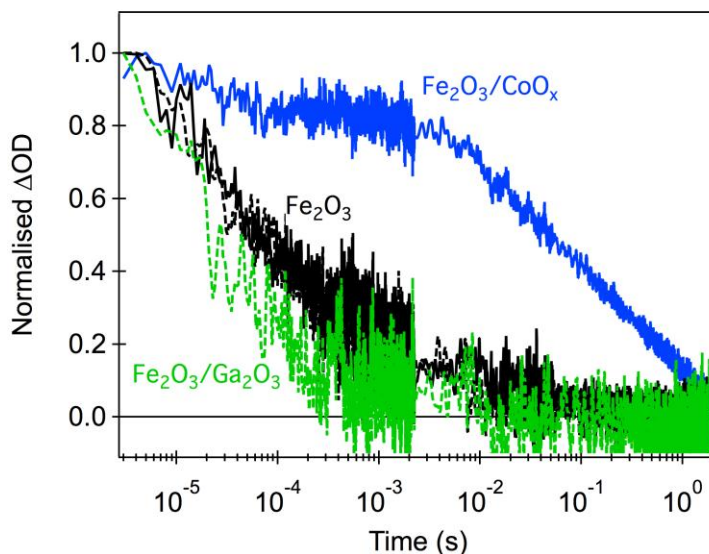


**Figure 2.** Normalised transient absorption decays of hematite photoholes probed at 700 nm and obtained with front-side low-intensity UV illumination (355 nm, 0.2 mJ/cm<sup>2</sup>, 0.33 Hz) of isolated hematite photoanodes, immersed in 0.1 M NaOH aqueous solution. Bare Fe<sub>2</sub>O<sub>3</sub> films are shown in black, Fe<sub>2</sub>O<sub>3</sub>/CoO<sub>x</sub> is shown in blue and Fe<sub>2</sub>O<sub>3</sub>/Ga<sub>2</sub>O<sub>3</sub> is shown in green. Decay traces corresponding to APCVD hematite are depicted with full lines and to USP hematite with dashed lines.

Figure 3 shows the corresponding dynamics of photogenerated hole absorption at 700 nm for the mesoporous hematite electrodes before and after modification, as a function of applied bias. In both cases, for the untreated electrodes (Figures 3a and 3c) it is apparent that at sufficiently anodic bias the hole decay dynamics become biphasic. The fast phase (lifetime up to ~ 10 ms) is assigned to electron / hole recombination.<sup>(39)</sup> The lifetime of this decay phase is retarded under high anodic bias conditions, assigned as previously to slower electron / hole recombination due to enhanced electron depletion in the photoelectrode at such bias conditions.<sup>(39)</sup> In addition, a slow (~ 2 second) decay phase is observed, assigned to long-lived holes, whose amplitude increases with increasingly anodic bias. The different magnitudes of the transient absorption signals from APCVD and USP photoelectrodes is related to the lower optical density of the USP hematite film, resulting in lower absorption of the excitation pulse.



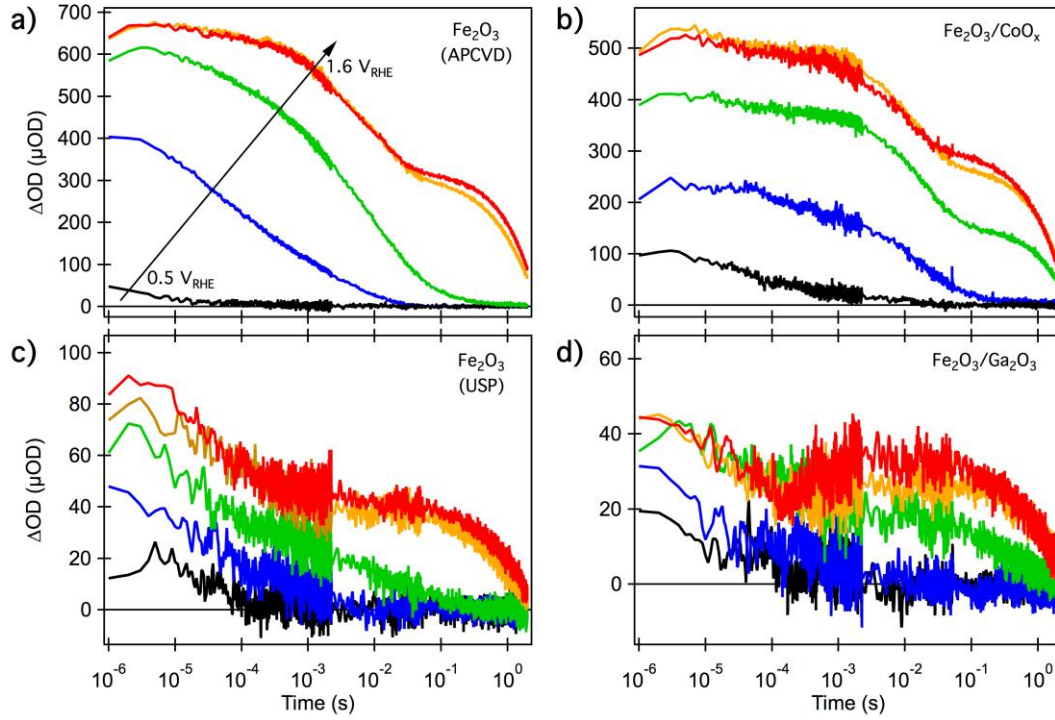


**Figure 3.** Electrical bias dependence of transient absorption decays probed at 700 nm following excitation at 355 nm of bare (left column, a and c) and treated (right column, b and d)  $\text{Fe}_2\text{O}_3$  photoanodes. The right column shows the effect of surface modification of the photoanodes with  $\text{CoO}_x$  (top, b) and  $\text{Ga}_2\text{O}_3$  (bottom, d). The applied potentials shown in the figures are 0.5  $V_{\text{RHE}}$  (black), 0.8  $V_{\text{RHE}}$  (blue), 1.1  $V_{\text{RHE}}$  (green), 1.4  $V_{\text{RHE}}$  (orange) and 1.6  $V_{\text{RHE}}$  (red).  $V_{\text{RHE}}$  represents the applied potential relative to the reversible hydrogen electrode (RHE).

We have previously shown that the amplitude of the long-lived hole signal correlates with photocurrent density for both  $\text{TiO}_2$  and hematite photoelectrodes without surface modifications.<sup>(34, 39)</sup> Qualitatively similar, biphasic decays were observed for the nanostructured APCVD hematite before and after  $\text{CoO}_x$  treatment (Figure 3a and 3b) and for the ultrathin USP hematite without and with  $\text{Ga}_2\text{O}_3$  overlayer (Figures 3c and 3d). However, quantitative analysis shows a striking shift in the bias dependence of the amplitude of the long-lived hole signal – with for example the data at 1.1  $V_{\text{RHE}}$  applied bias in Figure 3 showing negligible long-lived holes in the absence of surface modification, but a clear long-lived hole signal in the presence of  $\text{CoO}_x$  or  $\text{Ga}_2\text{O}_3$ .

Figure 4 plots the amplitude of the long-lived (2 second lifetime) hole signal as a function of applied bias for the electrodes studied herein. It is apparent that the  $\text{CoO}_x$

and  $\text{Ga}_2\text{O}_3$  treatments result, respectively, in a  $\sim 150 \pm 50$  mV and  $100 \pm 25$  mV cathodic shift of the appearance of these long-lived holes. This cathodic shift of long-lived hole generation correlates well with the cathodic shift of photocurrent generation observed above.(34, 39) It is striking that the two surface treatments result in very different effects on the charge carrier dynamics in the absence of applied bias, but rather similar effects under applied bias. The origin of this behaviour will be discussed below.

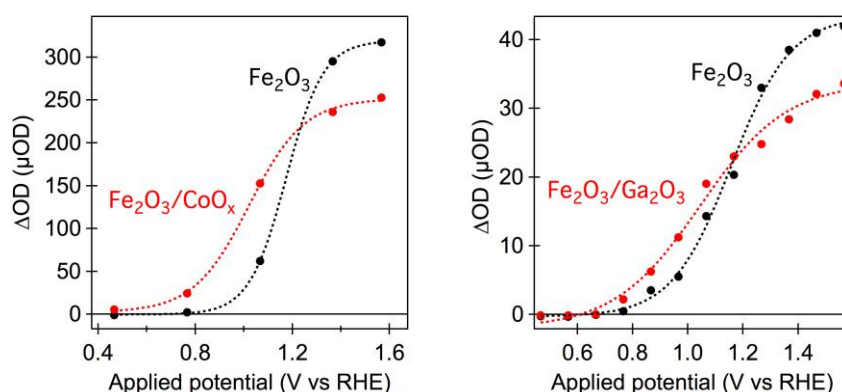


**Figure 4.** Amplitude of the 700 nm transient absorption measured at 50 ms after laser excitation, as a function of applied bias, for APCVD hematite before and after surface modification with  $\text{CoO}_x$  (left) and for ultrathin USP hematite before and after surface modification with  $\text{Ga}_2\text{O}_3$  (right). The dotted lines are intended to guide the eye and are not fits to a specific model.

We turn now to other signatures of the influence of surface treatment upon the photoelectrode activity as a function of applied bias, focusing in particular upon the  $\text{CoO}_x$  treatment. Figure 5 shows spectroelectrochemical data for a hematite photoanode without and with  $\text{CoO}_x$  treatment, plotting the change in UV/visible absorption as a function of increasingly anodic applied bias. For the untreated film, anodic bias is observed to result in the appearance of a well-defined positive absorption band at 580 nm. This positive absorption band is assigned to absorption of localised intra-bandgap states. Its observation for applied potentials only mildly positive of the  $\text{Fe}_2\text{O}_3$  conduction band suggests these states lie a few hundred millivolts below the conduction band. The observation of a positive absorption with increasing positive applied bias indicates that it derives from the oxidised form of this intraband redox state. The nature and function of these states will be discussed further

below. For the  $\text{CoO}_x$  treated film, the appearance of this 580 nm absorption band under anodic bias is superimposed upon a broader positive absorption, assigned to the oxidation of cobalt II or III ions present in the  $\text{CoO}_x$  layer.<sup>(40)</sup> Of particular interest to this paper is the bias dependence of the appearance of the 580 nm absorption feature, as plotted in Figure 5c. It is apparent that  $\text{CoO}_x$  treatment results in a  $\sim 100$  mV cathodic shift in the bias dependence of this feature, analogous to the cathodic shifts of the photocurrent and long-lived hole signals reported above.

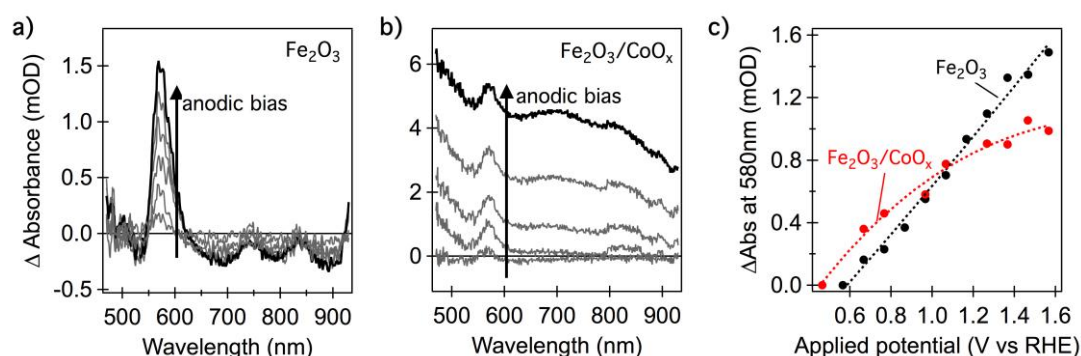


**Figure 5.** Spectroelectrochemistry of hematite photoanodes. a) Difference absorption spectra of a bare hematite photoanode measured at various potential biases in the range 0.7 V - 1.6 V relative to 0.6 V vs RHE; b) Difference absorption spectra of a  $\text{Fe}_2\text{O}_3/\text{CoO}_x$  photoanode measured at various potential biases in the range 0.6 V - 1.6V relative to 0.5 vs RHE. c) Absorption difference measured at 580 nm as a function of applied bias for the bare hematite photoanode (black) and the  $\text{Fe}_2\text{O}_3/\text{CoO}_x$  photoanode (red). The dotted lines are intended to guide the eye and are not fits to a specific model.

Finally we consider the full transient absorption spectral response of APCVD  $\text{Fe}_2\text{O}_3$  with and without  $\text{CoO}_x$  overlayer as a function of applied bias. Figure 6 summarises the transient absorption features observed between 500 and 900 nm for bare and  $\text{CoO}_x$ -treated films at four different applied biases. The colour coding in the figure corresponds to spectra measured at different time delays, ranging from 1  $\mu\text{s}$  (grey) to 2 s (red). It is apparent that the application of high anodic bias results in the generation of a broad, long-lived absorption with a maximum at  $\sim 650$  nm, apparent from the spectra at time delays of 100 ms – 2 s under 1.6  $\text{V}_{\text{RHE}}$  (Figure 6d), and evidenced also in Figure 6e. The spectrum of this broad signal is independent of  $\text{CoO}_x$  treatment, and distinct from the absorption increase assigned to cobalt oxidation

observed in the spectroelectrochemical data above. It is therefore assigned, as discussed previously,(32, 39) to hematite holes. In contrast to our previous studies in the absence of applied bias,(20) with bias control no long-lived bleaching signal is observed. This bleach was assigned previously to bleaching of cobalt oxide ground state absorption.

The broad, long-lived signal assigned to  $\text{Fe}_2\text{O}_3$  holes is apparent at a bias of 1.1  $V_{\text{RHE}}$  in  $\text{Fe}_2\text{O}_3/\text{CoO}_x$ , but is not observed at this voltage in the untreated hematite photoelectrode (Figure 6c), consistent with the cathodic shift of appearance of this long-lived hole signal discussed above. The spectral signature of long-lived holes in hematite is shown in Figure 6e, measured 1 s after laser excitation under various applied bias, in  $\text{Fe}_2\text{O}_3$  and  $\text{Fe}_2\text{O}_3/\text{CoO}_x$  electrodes. It is apparent that  $\text{CoO}_x$  treatment causes a cathodic shift in the appearance of this long lived signal, but does not significantly change its shape, confirming that for both the treated and untreated films, this long lived signal derives from hematite holes. Similarly the decay dynamics of this long-lived signal, and indeed the full spectral data observed under strong anodic bias (Figure 6d) are all independent of  $\text{CoO}_x$  treatment. We therefore conclude that whilst  $\text{CoO}_x$  does change the bias dependence of the yield of hematite holes, it does not change the lifetime of these transients.

Superimposed upon the broad, long-lived, hematite hole absorption, more complex behaviour is observed at earlier times (up to  $\sim 100$  ms) between 500 and 600 nm. In particular, a relatively intense, narrow absorption feature is observed peaking at  $\sim 580$  nm, as well as a smaller feature peaking at  $\sim 540$  nm for intermediate biases. Both of these features have largely disappeared by 100 ms in the potential range investigated. Under cathodic bias in the absence of  $\text{CoO}_x$ , the 580 nm band corresponds to a positive transient absorption increase. Both  $\text{CoO}_x$  treatment and more positive applied bias result in a progressive inversion of this feature, leading to a large absorption bleach peaking at 580 nm, whose magnitude increases with increasingly positive bias.

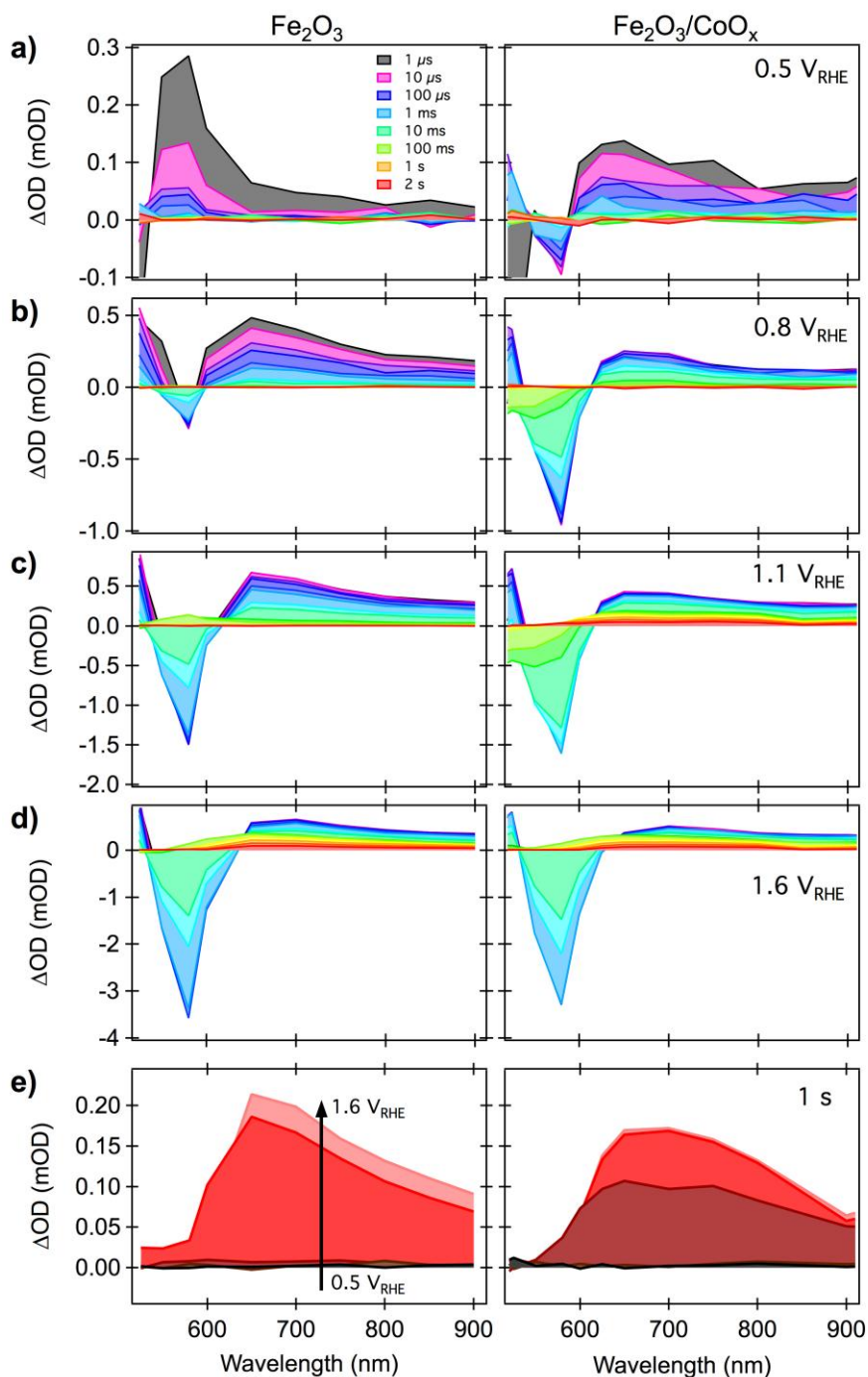


**Figure 6.** Time evolution of the transient absorption spectra of  $\text{Fe}_2\text{O}_3$  (left column) and  $\text{Fe}_2\text{O}_3/\text{CoO}_x$  (right column) photoelectrodes, under external applied bias: a)  $0.5 V_{\text{RHE}}$ , b)  $0.8 V_{\text{RHE}}$ , c)  $1.1 V_{\text{RHE}}$  and d)  $1.6 V_{\text{RHE}}$ , as indicated. e) Bias dependence of the appearance of long-lived hematite photoholes, probed at 1 s after laser excitation.

The 580 nm absorption feature observed in our transient absorption studies (either in isolated electrodes or those under external bias control) is assigned to the same intra-bandgap state absorption observed in our spectroelectrochemical data discussed above

and shown in Figure 5. Following that discussion, the positive transient feature observed at 580 nm for negative bias in the absence of  $\text{CoO}_x$  is assigned to oxidation of pre-reduced intraband states – corresponding, in this case, to hole trapping. This positive feature was also observed in absence of applied bias, and was most pronounced in undoped  $\text{Fe}_2\text{O}_3$  films, such as those used in our previous study of hole dynamics as a function of applied bias.(20, 32) Under anodic bias, these intraband states become increasingly pre-oxidised. As such, these states function increasingly as electron traps, becoming transiently reduced following the laser pulse, and generating the observed transient absorption bleach. We note that this 580 nm transient absorption feature decays completely in  $\sim 10$  ms, two orders of magnitude faster than the decay of the long-lived holes assigned to water oxidation. The decay of this feature does not correlate with a loss of hole absorption on the same timescale. As such, this 580 nm is assigned to defect states lying a few hundred meV below the  $\text{Fe}_2\text{O}_3$  conduction band.

## Discussion

Water photo-oxidation is a kinetically and thermodynamically difficult process. The concerted oxidation of two molecules of water to give one molecule of oxygen requires four holes (or ‘oxidising equivalents’), and as such is strongly dependent upon the presence of suitably catalytic sites to enable this multi-electron chemistry.(41) There is now extensive progress in the synthesis of molecular species capable of catalysing this multi-electron chemistry.(42, 43) Alternatively, photogenerated holes can oxidise water via a series of sequential one-hole oxidation reactions. These one-hole reactions are thermodynamically less favourable but do not require the accumulation of multiple oxidising equivalents at a catalytic site. Our previous study of the activation energy for the lifetime of the reaction of photogenerated hematite holes with water suggested that photogenerated holes on  $\text{Fe}_2\text{O}_3$  primarily oxidise water via a series of one-hole oxidation reactions.(35) We obtained further support for this conclusion from our observation that the kinetics of this oxidation reaction, and the overall photocurrent generation efficiency, were independent of light intensity and therefore hole density.(39) This sequential reaction pathway is most probably enabled by the highly oxidising nature of hematite valence band holes, and suggests that water photo-oxidation by hematite can proceed without the presence of specific catalytic sites for concerted multi-electron water

oxidation.(35) As such, it is plausible that the efficiency of water oxidation by hematite photoelectrodes may not be strongly dependent upon the introduction of catalytic water oxidation sites on its surface, such as those expected to be generated by the  $V_{\text{RHE}}$  treatment employed herein. We note that this lack of requirement for catalytic sites results from the highly oxidising nature of hematite photoholes; for photoelectrodes with less oxidising valence bands, the introduction of catalytic sites can be expected to be critical to achieve efficient water photooxidation.

From our previous work, it appears that a key requirement for water photo-oxidation by holes in hematite is that light absorption must generate these carriers with sufficient lifetime to be able to oxidise water. (33) Our transient kinetic studies also suggest that the lifetime required for water oxidation by hematite photoholes is on the order of one second, a conclusion supported by recent frequency domain photoelectrochemical analyses.(24) In particular, we observe here a close correlation between the bias dependence of the appearance of the long-lived photohole transient signal and the bias requirement for the observation of anodic photocurrents, providing further confirmation of requirement of long-lived holes to enable water oxidation. In this regard, the intrinsic n-type nature of these photoelectrodes may constitute a key limitation to their performance. This intrinsic n-doping is often further increased by the addition of extrinsic dopants such as silicon ions, added in part to improve the electron conductivity of such films so as to allow efficient electron collection by the external circuit,(22) but resulting also in a significant electron density within the film. As such, photogenerated holes are minority carriers, exhibiting rather short lifetimes and hole diffusion lengths (with the latter thought to be further reduced by a low hole mobility). This n-doping, and resultant rapid electron / hole recombination explains, at least in part, the requirement for the application of a high anodic bias to these films to reduce the electron density, with this electron depletion developing primarily adjacent to the electrode surface (depending upon the relative length scales of the depletion depth and film/particle size). This results in an increase in the hole diffusion length and the accumulation of long lived holes, which are able to oxidise water.

The observation of a cathodic shift in the bias dependence of water oxidation photocurrents upon the deposition of  $\text{CoO}_x$  on hematite, as well as with other cobalt treatments (most likely also conducive to the formation of related  $\text{CoO}_x$  layers), was

initially assigned, at least in part, to catalytic function of the cobalt-based layer in accelerating water oxidation.(26) In the studies we report herein, and previously,(2, 20) we find no evidence to support this conclusion. Our spectroelectrochemical studies show evidence of cobalt oxidation under positive applied bias for the  $\text{CoO}_x$  treated film. However, our transient studies indicate that the lifetime of long-lived photogenerated  $\text{Fe}_2\text{O}_3$  holes is independent of  $\text{CoO}_x$ , and in operating conditions (studies under bias control) show no evidence for the transfer of photogenerated hematite holes to the cobalt-based overlayer. A similar conclusion was recently reported for hematite films with  $\text{Co}^{2+}$  ions adsorbed at the hematite surface.(44) As such, whilst it has been widely reported that  $\text{CoO}_x$  deposited on conducting substrates such as ITO from  $\text{Co(II)}$  salts in phosphate buffer is an effective electrocatalyst, reducing the overpotential required for electrochemical water oxidation,(38) the cathodic shifts of photocurrent generation by hematite photoelectrodes induced by cobalt-based treatments do not appear to result primarily from this catalytic function. It is therefore necessary to consider alternative explanations for the enhanced photoelectrochemical performance.

Several studies have suggested that the cathodic shift of photocurrent generation by  $\text{CoO}_x$  and other treatments such as with  $\text{Ga}_2\text{O}_3$  or  $\text{Al}_2\text{O}_3$  overlayers may result from passivation of surface recombination sites, thereby partially suppressing surface recombination.(17, 25, 26) We note that there is some ambiguity in the nature of these “surface states”, and particularly whether this term refers only to states at the molecular scale electrode-electrolyte interface or also includes a finite region extending into the semiconductor (e.g. the space charge layer). There is extensive previous literature on the presence of intraband bulk traps and surface states on hematite, and their potential role as recombination centres.(30, 31, 45) In this regard, it is of particular note that the  $\text{Ga}_2\text{O}_3$  treatment reported herein did not result in a significant retardation of electron / hole recombination in the absence of applied bias – suggesting that whilst this treatment may well passivate surface states, this passivation alone is not sufficient to significantly influence electron / hole recombination.

A related explanation for the photocurrent onset shifts observed following both  $\text{CoO}_x$  and  $\text{Ga}_2\text{O}_3$  treatments is that they may influence the electron density in the  $\text{Fe}_2\text{O}_3$



photoelectrode, thereby retarding electron / hole recombination. We have previously attributed the increase in hole lifetime in the absence of applied bias following surface modification with  $\text{CoO}_x$  to such a decrease in electron density.<sup>(20)</sup> In the absence of applied bias, the effect was assigned to the oxidising nature of the surface modification that resulted in the development of a partial electron depletion of the  $\text{Fe}_2\text{O}_3$ , indicative of the formation of the  $\text{Fe}_2\text{O}_3/\text{CoO}_x$  heterojunction. This assignment is consistent with lack of any increase in hole lifetime following  $\text{Ga}_2\text{O}_3$  treatment; this treatment involves a deposition of a redox inactive oxide layer, and therefore would not be expected to result in electron depletion in the hematite film.

Enhanced electron depletion of the  $\text{Fe}_2\text{O}_3$  can also be invoked to explain the behaviour of photoanodes under operating conditions (i.e. under external bias control). In the limit of strong cathodic bias, both the  $\text{CoO}_x$  and  $\text{Ga}_2\text{O}_3$  treated films exhibit rapid hole decay dynamics, indicative of rapid electron / hole recombination induced by the high electron densities present in the films at these potentials. As the bias is shifted increasingly anodic, electron / hole recombination is retarded, leading to the formation of long-lived holes. The cathodic shift of the appearance of long-lived holes observed following  $\text{CoO}_x$  and  $\text{Ga}_2\text{O}_3$  treatments can thus be attributed to a cathodic shift in the development of electron depletion in the  $\text{Fe}_2\text{O}_3$ . Further support for such a shift can be obtained from our spectroelectrochemical data for the 580 nm absorption feature assigned to localised intra-band states of the  $\text{Fe}_2\text{O}_3$ . The magnitude of this signal can be used as an indicator of the redox occupancy of these states, and thus of the photoanode's Fermi level relative to the  $\text{Fe}_2\text{O}_3$  conduction band. In this regard, it is striking that the spectroelectrochemical data shows a cathodic shift of the 580 nm absorption signal in the presence of  $\text{CoO}_x$  (Figure 5c), indicating an increased electron depletion of the film following this surface modification.

It follows from the above arguments that the most likely origin of the cathodic shifts in photocurrent onset observed following both  $\text{CoO}_x$  and  $\text{Ga}_2\text{O}_3$  treatments is a reduced electron density in the hematite, reducing electron / hole recombination and increasing the yield of long-lived holes accumulating at the electrode surface. Such increased electron depletion following the  $\text{CoO}_x$  and  $\text{Ga}_2\text{O}_3$  treatments most likely results from surface state passivation, in agreement with several previous reports.<sup>(17, 25, 26)</sup> The presence of high densities of surface states causes Fermi level pinning at

the energies corresponding to such states, and a consequent decrease in the space charge layer width. Passivation of these states (i.e.: removal from the bandgap rather than just oxidation/reduction) will enhance electron depletion within the film for a given bias, consistent with the results reported herein. We note that the enhanced electron depletion observed following  $\text{CoO}_x$  treatment is also likely to be associated, at least in part, with the redox active nature of the cobalt oxide layer, as we have discussed previously (in the absence of applied bias, this is most probably the dominant cause of the slower electron / hole recombination observed following  $\text{CoO}_x$  treatment).(20) We conclude that these surface treatments result in a cathodic shift of the photocurrent, not primarily by removing surface recombination centres or enhancing the kinetics of water photo-oxidation, but rather by enhancing the spatial extent or magnitude of the space charge / electron depletion layer. As such, these results emphasise that one materials design strategy to enhance performance of water oxidation photoanodes, particularly those whose efficiency is limited by electron-hole recombination losses, is to target specifically the enhancement of electron depletion within the photoelectrode, whilst still ensuring sufficient conductivity through the film to allow electron extraction without large ohmic losses. Such strategies could include not only surface modification, as reported herein and extensively employed in the literature, but also strategies to enable efficient electron conduction without the requirement for chemical doping, such as core / shell and related architectures.(14)

## **Materials and Methods**

All the solvents and chemicals, unless otherwise stated, were obtained from Sigma-Aldrich or their subsidiaries and were used without further purification. Aqueous solutions were prepared with purified water (Millipore Corp., 18.2 M $\Omega$ cm at 25 °C). All experiments were performed at room temperature.

Si- doped  $\alpha\text{-Fe}_2\text{O}_3$  photoelectrodes were deposited on fluorine-doped tin oxide (FTO) by atmospheric pressure chemical vapour deposition (APCVD) and ultrasonic spray pyrolysis (USP) as described elsewhere(22, 25). Surface modification of hematite photoanodes with  $\text{CoO}_x$  and  $\text{Ga}_2\text{O}_3$  were carried out as described previously.(20, 25) Further details on electrode preparation and surface modifications are given in the Supporting Information.

Photoelectrochemical studies were carried out in a single-compartment, home-made PEC cell, in a three-electrode configuration with Ag/AgCl/0.3M NaCl (SSC) as reference electrode, Pt gauze as counter electrode and the hematite photoanode as working electrode, as reported previously(39) and detailed in the Supporting Information. The electrolyte solution employed was aqueous 0.1 M NaOH (pH 12.6).

All the applied potentials reported in this work are relative to the reversible hydrogen electrode (RHE). These values are obtained from those relative to the SSC using the Nernst equation:  $E_{\text{RHE}} = E_{\text{SSC}}^0 + E_{\text{SSC}} + 0.059\text{pH}$ , where  $E_{\text{SSC}}^0$  is the standard potential of the SSC reference (0.21 V<sub>RHE</sub> at 25 °C), and  $E_{\text{SSC}}$  is the potential measured versus the SSC.

The transient absorption setup has been described previously(34) and is detailed in the Supporting Information. Briefly, measurements on the  $\mu\text{s}$ -s time scale were obtained using the third harmonic of a Nd:YAG laser (Continuum Surelite I-10, at 355 nm, 6 ns pulse width) as excitation source, with laser intensity of  $0.20 \pm 0.02 \text{ mJ cm}^{-2}$  and repetition rate of 0.33Hz. Hematite photoanodes were placed in a sealed quartz cuvette filled with electrolyte solution (0.1 M NaOH) for the studies on isolated electrodes and in a home-made, two-compartment three-electrode PEC cell with borosilicate windows, for studies under applied bias.

## Acknowledgements

We thank Dr Christopher Barnett for equipment development and maintenance and SocMan Ho Kimura for lab support. Helpful discussions with Dr Piers Barnes are gratefully acknowledged. Financial support from the EPSRC the Swiss Federal Office of Energy (Project number 102326, PECHouse), and the European Commission's Framework Project 7 (NanoPEC, Project 227179) are gratefully acknowledged.

## References

1. Fujishima A & Honda K (1972) Electrochemical Photolysis of Water at a Semiconductor Electrode. *Nature* 238:37-38.
2. Bard AJ & Fox MA (1995) Artificial Photosynthesis: Solar Splitting of Water to Hydrogen and Oxygen. *Acc. Chem. Res.* 28:141-145.
3. Gratzel M (2001) Photoelectrochemical cells. *Nature* 414:338-344.

4. Walter MG, *et al.* (2010) Solar Water Splitting Cells. *Chem. Rev.* 110(11):6446-6473.
5. Osterloh FE (2008) Inorganic materials as catalysts for photochemical splitting of water. *Chem. Mater.* 20(1):35-54.
6. Kudo A & Miseki Y (2009) Heterogeneous photocatalyst materials for water splitting. *Chem Soc Rev* 38(1):253-278.
7. Maeda K (2011) Photocatalytic water splitting using semiconductor particles: History and recent developments. *J. Photochem. Photobiol. C: Photochem. Rev.* 12(4):237-268.
8. Bak T, Nowotny J, Rekas M, & Sorrell CC (2002) Photo-electrochemical hydrogen generation from water using solar energy. Materials-related aspects. *Int. J. Hydrogen Energy* 27(10):991-1022.
9. Santato C, Odziemkowski M, Ulmann M, & Augustynski J (2001) Crystallographically oriented Mesoporous WO<sub>3</sub> films: Synthesis, characterization, and applications. *J. Am. Chem. Soc.* 123(43):10639-10649.
10. Berglund SP, Flaherty DW, Hahn NT, Bard AJ, & Mullins CB (2011) Photoelectrochemical Oxidation of Water Using Nanostructured BiVO<sub>4</sub> Films. *J. Phys. Chem. C* 115(9):3794-3802.
11. Iwase A & Kudo A (2010) Photoelectrochemical water splitting using visible-light-responsive BiVO<sub>4</sub> fine particles prepared in an aqueous acetic acid solution. *J. Mater. Chem.* 20(35):7536-7542.
12. Sivula K, Le Formal F, & Grätzel M (2011) Solar Water Splitting: Progress Using Hematite (α-Fe<sub>2</sub>O<sub>3</sub>) Photoelectrodes. *ChemSusChem* 4:432-449.
13. Kronawitter CX, *et al.* (2011) A perspective on solar-driven water splitting with all-oxide hetero-nanostructures. *Energy & Environmental Science* 4(10):3889-3899.
14. Lin Y, Zhou S, Sheehan SW, & Wang D (2011) Nanonet-Based Hematite Heteronanostructures for Efficient Solar Water Splitting. *J. Am. Chem. Soc.* 133(8):2398-2401.
15. Zhong DK, Choi S, & Gamelin DR (2011) Near-Complete Suppression of Surface Recombination in Solar Photoelectrolysis by "Co-Pi" Catalyst-Modified W:BiVO<sub>4</sub>. *J. Am. Chem. Soc.* 133(45):18370-18377.
16. Steinmiller EMP & Choi KS (2009) Photochemical deposition of cobalt-based oxygen evolving catalyst on a semiconductor photoanode for solar oxygen production. *P Natl Acad Sci USA* 106(49):20633-20636.
17. Seabold JA & Choi K-S (2011) Effect of a Cobalt-Based Oxygen Evolution Catalyst on the Stability and the Selectivity of Photo-Oxidation Reactions of a WO<sub>3</sub> Photoanode. *Chem Mater* 23(5):1105-1112.
18. Zhong DK, Cornuz M, Sivula K, Gratzel M, & Gamelin DR (2011) Photo-assisted electrodeposition of cobalt-phosphate (Co-Pi) catalyst on hematite photoanodes for solar water oxidation. *Energy & Environ. Sci.* 4:1759.
19. McDonald KJ & Choi K-S (2011) Photodeposition of Co-Based Oxygen Evolution Catalysts on α-Fe<sub>2</sub>O<sub>3</sub> Photoanodes. *Chem Mater* 23(7):1686-1693.
20. Barroso M, *et al.* (2011) The Role of Cobalt Phosphate in Enhancing the Photocatalytic Activity of α-Fe<sub>2</sub>O<sub>3</sub> toward Water Oxidation. *J. Am. Chem. Soc.* 133(38):14868-14871.
21. Kanan MW, Surendranath Y, & Nocera DG (2009) Cobalt-phosphate oxygen-evolving compound. *Chem Soc Rev* 38(1):109-114.

22. Kay A, Cesar I, & Gratzel M (2006) New benchmark for water photooxidation by nanostructured  $\alpha$ -Fe<sub>2</sub>O<sub>3</sub> films. *J. Am. Chem. Soc.* 128(49):15714-15721.
23. Tilley SD, Cornuz M, Sivula K, & Grätzel M (2010) Light-Induced Water Splitting with Hematite: Improved Nanostructure and Iridium Oxide Catalysis. *Angew. Chem., Int. Ed.* 49(36):6405-6408.
24. Le Formal F, *et al.* (2011) Passivating surface states on water splitting hematite photoanodes with alumina overlayers. *Chem Sci* 2(4):737-743.
25. Hisatomi T, *et al.* (2011) Cathodic shift in onset potential of solar oxygen evolution on hematite by 13-group oxide overlayers. *Energy & Environ. Sci.* 4:2512-2515.
26. Spray RL, McDonald KJ, & Choi K-S (2011) Enhancing Photoresponse of Nanoparticulate  $\alpha$ -Fe<sub>2</sub>O<sub>3</sub> Electrodes by Surface Composition Tuning. *J. Phys. Chem. C* 115(8):3497-3506.
27. Gardner RFG, Tanner DW, & Sweerr F (1963) Electrical properties of alpha ferric oxide. 2. Ferric oxide of high purity. *J. Phys. Chem. Solids* 24:1183.
28. Ahmed SM, Leduc J, & Haller SF (1988) Photoelectrochemical and impedance characteristics of specular hematite. 1. Photoelectrochemical, parallel conductance, and trap rate studies. *J. Phys. Chem.* 92:6655.
29. Kennedy JH & Frese KW (1978) *J. Electrochem. Soc.* 125:709.
30. Dare-Edwards MP, Goodenough JB, Hamnett A, & Trelvellick PR (1983) Electrochemistry and Photoelectrochemistry of Iron(III) Oxide. *J. Chem. Soc., Faraday Trans.* 79:2027.
31. Sanchez C, Sieber KD, & Somorjai GA (1988) The Photoelectrochemistry of Niobium Doped Alpha-Fe<sub>2</sub>O<sub>3</sub>. *J Electroanal Chem* 252(2):269-290.
32. Pendlebury SR, *et al.* (2011) Dynamics of photogenerated holes in nanocrystalline [small alpha]-Fe<sub>2</sub>O<sub>3</sub> electrodes for water oxidation probed by transient absorption spectroscopy. *Chem. Comm.* 47(2):716-718.
33. Wijayantha KGU, Saremi-Yarahmadi S, & Peter LM (2011) Kinetics of oxygen evolution at  $\alpha$ -Fe<sub>2</sub>O<sub>3</sub> photoanodes: a study by photoelectrochemical impedance spectroscopy. *Phys Chem Chem Phys* 13(12):5264-5270.
34. Cowan AJ, Tang JW, Leng WH, Durrant JR, & Klug DR (2010) Water Splitting by Nanocrystalline TiO<sub>2</sub> in a Complete Photoelectrochemical Cell Exhibits Efficiencies Limited by Charge Recombination. *J Phys Chem C* 114(9):4208-4214.
35. Cowan AJ, *et al.* (2011) Activation Energies for the Rate-Limiting Step in Water Photooxidation by Nanostructured  $\alpha$ -Fe<sub>2</sub>O<sub>3</sub> and TiO<sub>2</sub>. *J. Am. Chem. Soc.* 133(26):10134-10140.
36. Pesci FM, Cowan AJ, Alexander BD, Durrant JR, & Klug DR (2011) Charge Carrier Dynamics on Mesoporous WO<sub>3</sub> during Water Splitting. *J Phys. Chem. Lett.* 2(15):1900-1903.
37. Le Formal F, Gratzel M, & Sivula K (2010) Controlling Photoactivity in Ultrathin Hematite Films for Solar Water-Splitting. *Adv Funct Mater* 20(7):1099-1107.
38. Kanan MW & Nocera DG (2008) In situ formation of an oxygen-evolving catalyst in neutral water containing phosphate and Co<sup>2+</sup>. *Science* 321(5892):1072-1075.

39. Pendlebury SR, *et al.* (2012) Correlating long-lived photogenerated hole populations with photocurrent densities in hematite water oxidation photoanodes. *Energy & Environ. Sci.*
40. Dafonseca CNP, Depaoli MA, & Gorenstein A (1994) Electrochromism in Cobalt Oxide Thin-Films Grown by Anodic Electroprecipitation. *Sol Energ Mat Sol C* 33(1):73-81.
41. Dau H, *et al.* (2010) The Mechanism of Water Oxidation: From Electrolysis via Homogeneous to Biological Catalysis. *Chemcatchem* 2(7):724-761.
42. Yagi M & Kaneko M (2000) Molecular Catalysts for Water Oxidation. *Chemical Reviews* 101(1):21-36.
43. Llobet A (2010) Catalytic water oxidation: Rugged water-oxidation anodes. *Nat Chem* 2(10):804-805.
44. Upul Wijayantha KG, Saremi-Yarahmadi S, & Peter LM (2011) Kinetics of oxygen evolution at [small alpha]-Fe<sub>2</sub>O<sub>3</sub> photoanodes: a study by photoelectrochemical impedance spectroscopy. *Phys Chem Chem Phys* 13(12):5264-5270.
45. Horowitz G (1983) Capacitance Voltage Measurements and Flat-Band Potential Determination on Zr-Doped Alpha-Fe<sub>2</sub>O<sub>3</sub> Single-Crystal Electrodes. *J Electroanal Chem* 159(2):421-436.